TELECOM INFRA PROJECT

Analysis of 28GHz and 60GHz Channel Measurements in an Indoor Environment

Table of Contents

1. Introduction

The mmWave spectrum (30GHz - 300GHz) is a subset of the electromagnetic spectrum that is increasingly being adopted for use in high speed wireless communication. One motivation for choosing mmWave as the target for next generation systems is the significantly higher potential capacity than possible in sub-6 GHz networks. This is due to the availability of much larger channel bandwidth, and the ability to use beam forming for greater spatial reuse.

The 3GPP standard has chosen the 28GHz and 39GHz mmWave bands with the K_a band for next-generation 5G NR systems. The 60GHz band within the V-band is standardized through IEEE's 802.11ad and 802.11ay. A motivation for developing technologies at 60GHz rather than 28GHz or 39GHz is the abundance of available unlicensed spectrum in the V-band in many regions around the globe.

In this paper, we will discuss the side-by-side characterization of propagation in both the 28GHz and 60GHz bands to develop an understanding of losses through common materials encountered in typical deployments. In addition, we compare the losses of reflection from surfaces of common materials, to build an understanding of potential for deployment where Non-Line of Sight (NLOS) links can be utilized through reflections for communication.

This white paper has been composed by the engineering team from Facebook and has been contributed to the mmWave Project Group of Telecom Infra Project (TIP) under the Channel Modeling track. More information on TIP can be found at [1] and on the mmWave Project Group at [2].

2. Motivation

Design of the next generation of mmWave communication systems requires a detailed characterization of the propagation channel. It is well understood by radio engineers that different frequency bands have unique characteristics that affect link performance. Indeed, the large range in regulations and radio products across wireless communication bands are reflective of such differences.

A major challenge of mmWave communication is overcoming atmospheric absorption losses at high frequencies. While the 60GHz channel offers even more contiguous bands (up to 2GHz) compared to the 28GHz band, the absorption spectrum of oxygen has a resonant peak at 60GHz, and propagation at 60GHz suffers from high levels of atmospheric absorption up to 16dB/km in free space, and approximately an additional 21dB/km in the rain [6].

To avoid additional losses, mmWave links are typically deployed with a clear line of sight (LOS) path. In a given deployment, there may be multiple potential non-line of sight (NLOS) paths of significant signal strength due to reflections. Urban environments contain many objects – buildings, roadways, vehicles, trees – that influence the propagation of radio frequency signals, and an understanding of the potential advantages and risks of deploying in such environments can help operators build more reliable wireless networks.

The results of this study would allow the designers to weigh the benefits (wider bandwidth) and challenges (higher loss) of the 60GHz channel against that of the 28GHz channel. The aim of this project is to characterize the 28GHz channel and compare the results to the 60GHz channel characterization obtained by similar sounder equipment, in an identical environment, with measurements made using a similar methodology.

The body of this paper is organized into five sections (in addition to Section 1, which describes the background of the study) in the following order: Section 3 outlines the channel sounding equipment for 60GHz and 28GHz along with a high-level description of the measurement procedure. Section 4 benchmarks the baseline performance for the 60GHz and 28GHz sounders and compares the measured values with theoretical free space path loss (FSPL) values. The reciprocity of the sounders is also compared in this section. Section 5 presents the measured transmission losses of common materials in an urban environment such as wood, drywall, glass and foliage (from trees and shrubbery). Section 6 details results of reflection losses over concrete, glass, wood and drywall. Results from publicly available comparative literature has also been provided in Sections 5 & 6. In Section 7, the results from the preceding sections have been summarized.

3. Equipment and Test Procedure

A common practice with new bands is to characterize the band through a series of channel measurements using specialized "channel sounders" that are typically custom systems costing >$250K each. Several research institutions have performed channel sounding experiments using such custom hardware in the 5G and 60GHz bands, although few have performed side-by-side channel comparisons.

In order to reduce cost, improve flexibility, and increase accessibility to channel sounder hardware, the TIP mmWave project group has launched a channel sounder initiative to develop a low-cost flexible solution based on Facebook's Terragraph (TG) hardware [8], operating at 60GHz. The Terragraph radios, running an automated channel sounder software package, are used for 60GHz propagation measurement in this study. The 28GHz channel sounder hardware is based on a custom hardware design. The specifications for both channel sounder systems used in this side-by-side study are summarized in Table 1, below.

Parameter	60GHz	28GHz
Array Dimensions	8x36	16x16
Half-power Beamwidth	2.8°	6.4°
Waveform	802.11ad (MCS1)	802.11ad (MCS1)
Center Frequency	60.48GHz	26.5GHz
Channel Bandwidth	2.16GHz	2.16GHz
Antenna Type	Patch + Waveguide	Patch
Antenna Polarization	Linear/Vertical	Linear/Vertical

Table 1: Comparison of the sounder hardware specifications and properties

Photographs of the two channel sounder antenna arrays that are used in this study are shown in Figure 1, below. In additional to laser-based alignment, both sets of phased array antennas are electrically steered from -45° to 45° with a step of 1.4° for both receiver and transmitter, such that the optimal LOS with minimum path loss is found between the sounder radios.

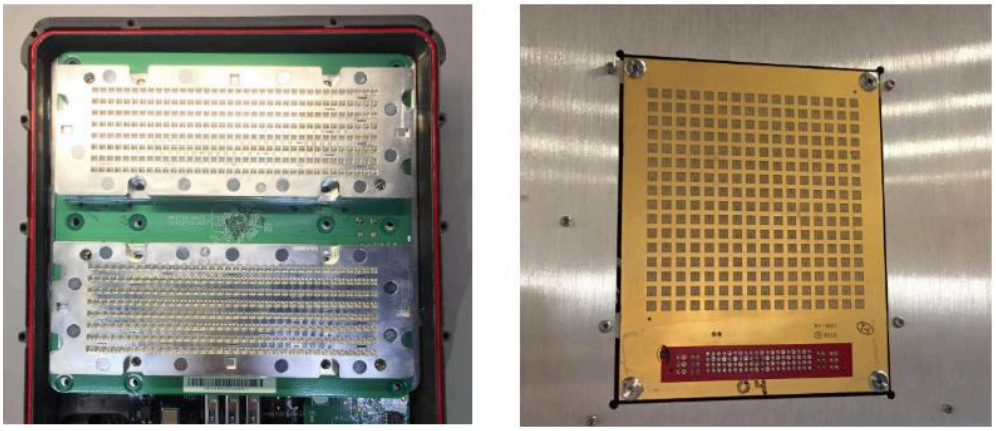

Figure 1: Photographs of the radios and antenna arrays for the 60GHz channel sounder (left). The 28GHz channel sounder (right) photo courtesy of Esencia Technologies, Inc.

3.1 60GHz Channel Sounder

The 60GHz channel sounder is based on the Terragraph hardware that has been developed at Facebook and adapted for channel propagation measurements through the TIP Channel Sounder initiative. Since the intended use of Terragraph is as a communication link rather than a measurement tool, an additional software platform has been developed for automated control and coordination of channel sounding measurements. To allow accurate measurement of physical properties of the electromagnetic channel, a series of additional calibration routines was performed on a per-unit basis.

The channel sounder is calibrated through the use of a calibrated National Instruments (NI) mmWave transceiver system to accurately report the absolute incident power, absolute effective isotropic radiated power (EIRP), and path loss between the receiver and transmitter. All measurements were performed in channel 2 of the 802.11ad standard (with center frequency of 60.48GHz). Calibration is performed over a range of temperatures, gain settings, and beam-steering angles.

Receiver Power Calibration

The measurement setup for receiver calibration is shown in Figure 2. The measurement is performed for the bore sight alignment between the transmitter horn antenna and the receiver antenna array. The alignment of units and distance measurement is performed using a laser.

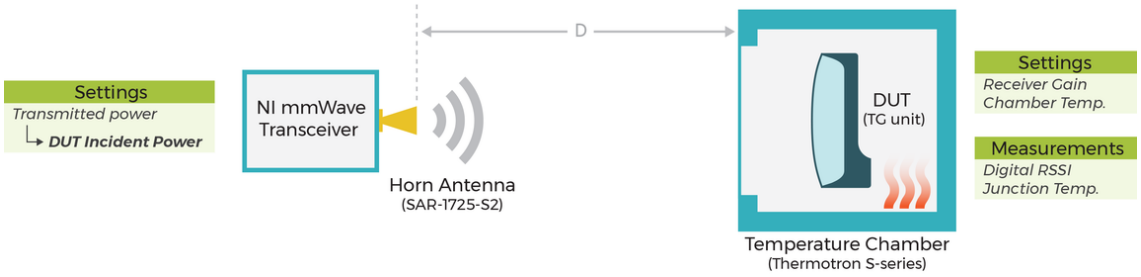

Figure 2: Diagram showing configuration for calibrating 60GHz receiver RSSI over incident power, settings, and temperature

The chipset used in the Terragraph radio provide digital $RSSI$ metrics that are calculated based on post-ADC data samples. Receiver gain settings are programable parameters as well as reportable by the chipset. A combination of digital (also known as raw) $RSSI$ and Receiver gain settings are used to estimate $RSSI$ at antenna input in dBm units.

The following equation represents the measurement relationships (powers in dBm and gains in dB):

$$EIRP - PL + g_{ANT} + g_{RX} = pRSSI$$

where $EIRP$ is the transmitter's effective isotropically radiated power, PL is the free space path loss, g_{ANT} is the antenna gain of the horn, g_{RX} is the combined receiver RF and IF gain, and p_{RSSI} is the $RSSI$ readout translated into dBm power. The tunable parameters are the $EIRP$ and receiver IF and RF gains (Rx_RF_ind, Rx_IF_ind). Antenna gain and path loss are given by the Friis equation:

$$PL = -27.55 + 20\,log\,F_c + 20\,log\,D$$

Where F_c is the center frequency in MHz and D is distance in meters. Direct calibration in terms of gain indices, $RSSI$ readout, and temperature T requires an explicit derivation of p_{RSSI} mapping and individual receiver gain calibrations. Moreover, receiver antenna gain is represented with antenna/slave selection setup, Rx_Ant_setup (see below). In summary, the true incident received power p_{RX} is given as:

$$p_{RX} = EIRP - PL = f(Rx\_RF\_ind, Rx\_IF\_ind, RSSI, T, Rx\_Ant\_setup)$$

The receiver calibration procedure involves characterizing $f()$ in a lookup table (LUT). To measure variations over temperature, each radio is placed inside a controlled temperature

chamber with the antenna elements exposed towards the transmitter horn antenna, as shown in the picture. The logged temperature used in channel sounding is the reported junction temperature from the RFIC rather than the programmed oven temperature.

The LUT is populated during the $RSSI$ calibration procedure. The absolute incident power, p_{RX}, is calculated as:

$$p_{RX} = EIRP - PL = p_{TX} + g_{HORN} + 27.55 - 20\,log(F_c) - 20\,log\,D$$

where p_{TX} is the signal generator transmit power and g_{HORN} is the horn antenna gain. Using this mapping of settings and $RSSI$ to p_{RX}, we find the nearest LUT entries for a given temperature and $RSSI$ and interpolate to find the absolute incident power on the receiver unit within a small margin of error.

Transmitter Power Calibration

Although a self-calibration mechanism for transmit power is implemented and utilized for normal operation of TG links, the accuracy of this built-in transmitter calibration method is not sufficient for the purpose of channel characterization. The accuracy of this built-in calibration further degrades at high and low temperatures. Furthermore, this built-in calibration only calibrates the PAs on-chip, without taking into account variations in antenna and PCB characteristics from board to board.

As a result, a comprehensive calibration of transmit power vs temperature and gain index is required to meet the 60GHz channel sounder targets. The measurement setup is shown in Figure 3.

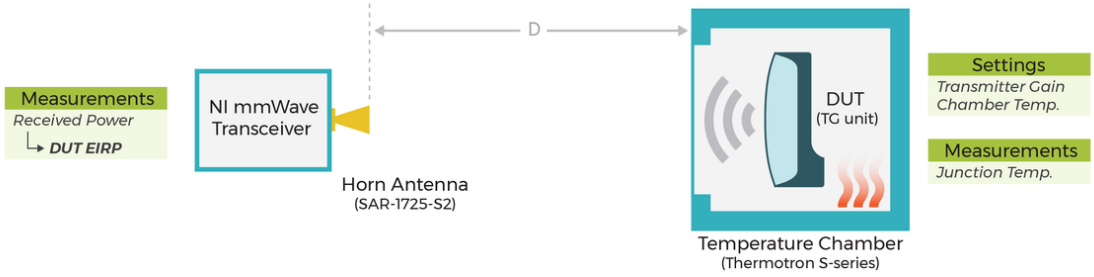

Figure 3: Diagram showing configuration for calibrating 60GHz transmitter EIRP over settings and temperature

The implemented measurement setup is similar to the $RSSI$ calibration with the roles of transmitter and receiver reversed. Each unit is placed into a temperature chamber with the calibration procedure repeated for several temperature points within the usage range. The

DUT's $EIRP$ is measured the a calibrated 60GHz receiver equipment, and the measured $EIRP$ is collected over all transmit power indices and temperature region of interest.

The calibration lookup table is populated during the transmit power calibration procedure. The transmit $EIRP$ is calculated as:

$$EIRP = p_{RX} - g_{HORN} + PL = p_{RX} - g_{HORN} - 27.55 + 10\,log\,F_c + 10\,log\,D$$

For both the receiver and transmitter look up tables, an automated post processing step is used in the channel sounding procedure to interpolate between temperature and measured receiver/transmitter metrics to obtain calibrated values for incident power, $EIRP$, and path loss.

3.2 28GHz Channel Sounder

The 28GHz channel sounder hardware is based on a modified 802.11ad modem, a custom designed 26.5GHz RF transceiver, and a 16x16 element phased-array antenna (PAA). Unlike the 60GHz channel sounder, every element of the 28GHz PAA is independently controllable and thus supports both azimuth and altitude beam scanning. To minimize the introduction of channel measurement errors resulting from differences in the 60GHz and 28GHz PAA architectures, each vertical row of antenna of the 28GHz PAA is programmed with identical phase and gain settings, restricting beam scanning to azimuth only.

While the 60GHz channel sounder unit employs a passive heatsink for thermal management, the 28GHz channel sounder has an integrated cooling fan. This provides an opportunity to improve precision of the receiver and transmitter gain settings by using the fan to stabilize the temperature inside the enclosure by controlling the fan speed. A simple proportional-integral-derivative (PID) loop modulates the fan speed using a pulse-width modulated (PWM) controller, while monitoring the temperature of the of the RF transceiver, to maintain the temperature RF transceiver at a programmed set point of 30C. The PWM controller and temperature measurement is very accurate which results in extremely consistent (receiver and transmitter gain control of < 1dB). However, this operates well only when ambient temperature is between 15-30 C. While this operates very well for indoor testing, outside of this temperature range the fan stops when the ambient temperature is too cool, and it is limited by the volume of air it can push through the system when it is too hot, resulting in Tx and Rx gain variation. To address this issue and support outdoor testing, the TX gain and RX gain of the RF transceiver is temperature compensated using a gain look-up-table (LUT) indexed with the temperature of the RF transceiver PCB. Likewise, the PAA antenna gain is adjusted using the case temperature of the PAA antenna. To create the LUTs, the enclosed unit, with fans, was placed in an environmental chamber and the TX and RX gain, the RF transceiver PCB

temperature, and phase-array antenna case temperature, was measured and logged as ambient temperature was varied from 0 to 45 C. This data was then modeled with a weighted interpolation polynomial so that Tx and Rx gain and Tx gain error (relative to measurements made at 25 C ambient) could be calculated.

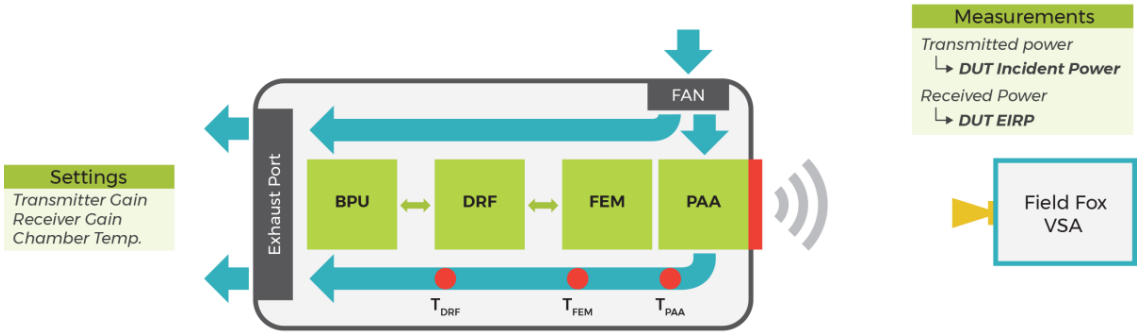

Figure 4: Diagram showing of temperature stabilization system

The TX gain LUT is used in real time to adjust TX attenuators. The RX compensation operates similarly. However, the gain compensation for the Rx transceiver, was implemented by post-processing the RX channel power indicator (RCPI) and RX PCB temperature data.

To further improve accuracy, At the start of each channel test, the TX EIRP is also measured using a reference TX horn and a calibrated power meter to confirm that TX EIRP of the reference is accurate and stable. The diagrams below illustrate the measurements described above.

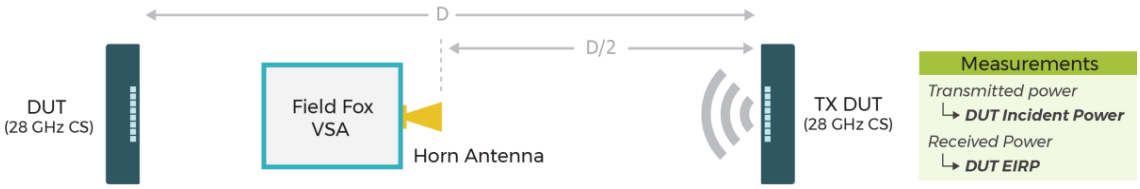

Figure 5: Diagram showing configuration for measuring stability 28GHz system in lab using reference horn and power meter

4. Baseline Measurements

To ensure that both channel sounders are reporting values that are repeatable and consistent with theory, several baseline measurements were performed before each set of measurements (summarized in Table 2, below). The baseline scenarios that are analyzed are (1) comparison of measured path loss to theoretical path loss, (2) repeatability of consecutive measurements, (3) reciprocity in path loss measurements.

It is well understood that losses associated with free-space propagation are frequency-dependent, and given by the Friis transmission equation:

$$FSPL = -27.55 + 20\,log\,F_c + 20\,log\,D$$

Since this frequency-dependent propagation loss is well understood and consistent, it is de-embedded from all reported measurements for the purpose of comparing losses exclusively from atmospheric effects and material properties. The frequency difference between the two center frequencies of the channel sounders accounts for 7.1dB additional path loss for free-space propagation loss at 60GHz.

	60GHz			
Description	**# of Samples**	**Theoretical FSPL (dB)**	**Measured FSPL (dB)**	**Δ (dB)**
FSPL at 4.6m distance	11	81.3	79.5	-1.8 ± 0.3
FSPL at 9.6m distance	30	87.7	85.4	-2.3 ± 1.0
FSPL at 9.6m distance (1 to 2)	15	87.7	85.4	-2.3 ± 1.3
FSPL at 9.6m distance (2 to 1)	15	87.7	85.4	-2.3 ± 0.8

Table 2: Summary of baseline free space measurements for 60GHz

The measured path loss values with both sets of channel sounders are within expectations given potential error sources during the calibration procedure and quantization error in reported digital RSSI. At a 10m distance, the average error in path loss measurements at 28GHz

is -0.5dB, and average error for 60GHz is -2.3dB. For both channel sounders the standard deviation in measurements is within about 1dB, indicating that measurements are reasonably repeatable.

	28GHz			
Description	**# of Samples**	**Theoretical FSPL (dB)**	**Measured FSPL (dB)**	**Δ (dB)**
FSPL at 4.6m distance	2	74.2	74.2	0.0 ± 0.0
FSPL at 9.6m distance	12	80.3	79.8	-0.5 ± 0.5
FSPL at 9.6m distance (1 to 2)	6	80.3	80.1	-0.2 ± 0.2
FSPL at 9.6m distance (2 to 1)	6	80.3	79.6	-0.7 ± 0.6

Table 3: Summary of baseline free space measurements for 28GHz

All subsequent loss measurements are reported relative to the measured path loss in each configuration. In this way, deviation from absolute path loss does not bias reported loss measurements, and the numbers reported are measured penetration losses within the 1dB of measurement standard deviation.

For both sounder systems, the path loss measurements are reciprocal (independent of link direction) and independent of transmit power as long as we are operating within the dynamic range of the receiving unit. Both units are also resistant to misalignment in the horizontal direction since we are performing 90 degrees of azimuth beam scan for each measurement and reporting the lowest measured path loss value.

5. Transmission Loss Measurements

Losses associated with transmission through building materials are important to understand for deployment in environments without clear LOS, between indoor and outdoor nodes, between rooms, or where the LOS path may be occasionally obstructed. In this section, we have characterized the path loss for a number of materials, with results summarized for each material.

A number of mmWave propagation measurement campaigns have been described in the literature prior to this study. This measurement campaign is the first to address propagation and reflection loss in both the 28GHz licensed and 60GHz unlicensed bands. It is also one of the first to use electronically steerable measurement equipment that has similar characteristics to the equipment that will be commercially deployed. The materials under test have been thoroughly described. Where possible, reference is made to data from previous campaigns for comparison. These comparisons are sometimes inexact due to the nature of the laboratory test equipment and imprecise descriptions of the material composition and dimensions.

5.1 Wood

Penetration loss through wood is a critical use case for indoor communication through walls and doors, and indoor-to-outdoor communication. We have evaluated penetration through three different types of plywood that are commonly employed in construction: 4 ply 12mm plywood, 7 ply 18mm plywood, and 12mm oriented strand board (OSB) (see Figure 6).

The measurements were conducted with radio transceivers separated by a 9.6m distance, with the wood panels placed at the midpoint between transceivers. In addition to characterizing the loss at normal incidence, the wood was also rotated to characterize loss at angled incidence, which are expected to have greater transmission loss. The summary of measurements for each of the wood types is shown in Tables 4, 5, and 6 below.

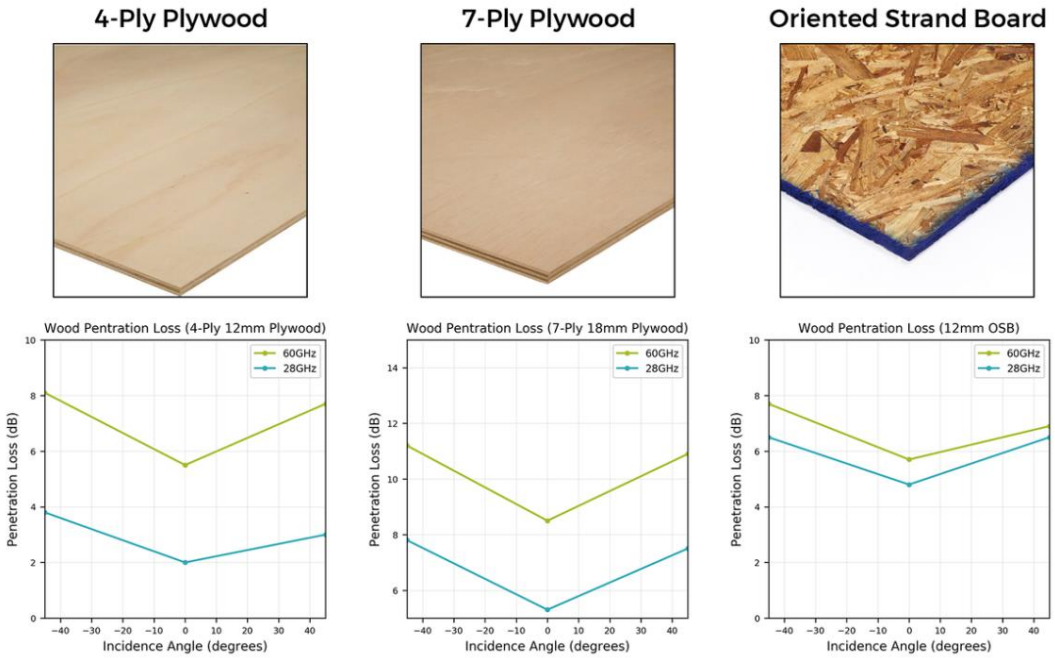

Figure 4: Penetration loss as a function of incidence angle is shown for 3 types of wood: 4-ply plywood (12mm), 7-ply plywood (18mm), and oriented strand board (12mm)

	60GHz		28GHz	
Description	**# of Samples**	**Loss (dB)**	**# of Samples**	**Loss (dB)**
4 Ply 12 mm Plywood - 0°	2	5.5 ± 0.7	2	6.8 ± 0.4
4 Ply 12 mm Plywood - 45°	4	7.7 ± 0.5	4	4.8 ± 0.4

Table 4: 12 mm plywood penetration loss average and standard deviation

	60GHz		28GHz	
Description	**# of Samples**	**Loss (dB)**	**# of Samples**	**Loss (dB)**
12 mm OSB - 0°	2	5.7 ± 0.8	2	4.8 ± 0.4
12 mm OSB - 45°	4	7.3 ± 0.6	4	6.5 ± 0.0

Table 5: 12 mm OSB penetration loss average and standard deviation

	60GHz		28GHz	
Description	**# of Samples**	**Loss (dB)**	**# of Samples**	**Loss (dB)**
Seven Ply 18 mm Plywood 0°	2	8.5 ± 0.4	2	5.3 ± 1.1
Seven Ply 18 mm Plywood 45°	4	11.1 ± 0.5	4	7.6 ± 0.5

Table 6: 18mm 7-ply plywood penetration loss average and standard deviation

The normalized loss for a normal angle of incidence for 4 ply wood is 4.6dB/cm for 60GHz and 1.7dB/cm for 28GHz; for 7 plywood it is 4.7dB/cm for 60GHz and 4.0dB/cm for 28GHz; and for OSB it is 4.7dB/cm for 60GHz and 2.9dB/cm for 28GHz. This gives an average loss of about 4.7dB/cm for 60GHz and 2.9dB/cm for 28GHz across all tested wood types.

The measurements of penetration loss for wood taken at 60GHz in this study are higher than the findings of some other campaigns. In "Propagation Characterization of an Office Building in the 60GHz Band" [3], Lu *et al* observed a penetration loss of 1.3dB/cm at 60GHz. Similarly, Fuschini *et al* in "Item level characterization of mm-wave indoor propagation" [10] reported a penetration loss of 2.1dB/cm at 60GHz. By contrast, Huang et al measured a transmission loss of 7.6dB/cm at 60GHz for plywood in "60GHz Transmission and Reflection Measurements" [7].

At 28GHz, the 5G Channel Model Special Interest Group reported a finding of a penetration loss of ~4dB/cm at 28GHz in their white paper "5G Channel Model for bands up to 100GHz" [10]. In "Characteristics Analysis of Reflection and Transmission According to Building Materials in the Millimeter Wave Band" [9], Choi *et al* reported a penetration loss for plywood of 5dB, averaged over measurements from 13GHz to 28GHz, and for wood of 13dB. These results correspond well with the findings in this study.

5.2 Drywall

As through-wall penetration enables a number of indoor mmWave use cases, we characterized the penetration loss of drywall, a primary component of wall constructions. Interior walls feature other components, such as wood and metal studs, but such geometries vary widely and have complex scattering behavior. For this reason, characterization on a per-material basis provides a better general understanding of propagation characteristics and gives sufficient information to estimate losses through a complete wall.

Since drywall is a relatively transparent material with low loss at mmWave frequencies, multiple layers of drywall had to be used in order to obtain a total loss measurement that is larger than the measurement error of the equipment (see Figure 8). The measurements for penetration losses through 1-4 layers of drywall are summarized in Figure 7 and Table 7, below.

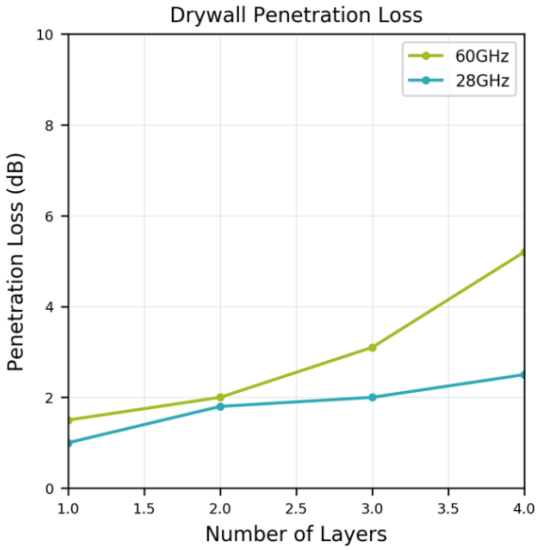

Figure 5: Measurement of penetration loss through drywall as a function of number of drywall layers

Figure 6: Photograph of measurement setup for multi-layer dry wall measurements

	60GHz		28GHz	
Description	**# of Samples**	**Loss (dB)**	**# of Samples**	**Loss (dB)**
Dry Wall - 1 Layer 12 mm 0°	2	1.5 ± 0.5	2	1.0 ± 0.0
Dry Wall - 2 Layers 24 mm 0°	2	2.0 ± 0.3	2	1.8 ± 0.4
Dry Wall - 3 Layers 36 mm 0°	2	3.1 ± 0.0	2	2.0 ± 0.0
Dry Wall - 4 Layers 48 mm 0°	2	5.2 ± 0.1	2	2.5 ± 0.0

Table 7: Dry Wall penetration losses with different number of layers and thicknesses

Average loss for a single layer of drywall is 1.19dB for 60Ghz, and 0.79dB for 28GHz. Standard deviations are 0.28dB and 0.18dB, respectively.

The measurements for drywall taken in this study compare well to the findings of other campaigns. In "28GHz millimeter wave cellular communication measurements for reflection and penetration loss in and around buildings in New York city" [4], Zhao *et al* measured attenuation through a wall composed of two sheets of drywall with an air gap of 7dB at 28GHz, equivalent to 2.8dB/cm. In their white paper "5G Channel Model for bands up to 100GHz" [10], the 5G Channel Model Special Interest Group reported a finding of a penetration loss of ~1.5dB/cm at 28GHz. Choi *et al* reported an average penetration loss of 4dB over measurements taken from 13GHz to 28GHz in "Characteristics Analysis of Reflection and Transmission According to Building Materials in the Millimeter Wave Band" [9]. Anderson *et al* reported in "In-Building Wideband Partition Loss Measurements at 2.5GHz and 60GHz" [5] a normalized penetration loss of 2.4dB/cm at 60GHz.

5.3 Glass

Penetration loss measurements were completed for two types of glass commonly used for windows in construction. "Glass #1"is low-emissivity double-pane window glass that is representative of glass commonly used in window interfacing between interiors and the outside. Each glass layer is 3.18 mm (1/8") thick, covered with a conductive silver film and separated by a 12.7 mm (1/2") Argon-gas-filled cavity. Characterizing losses through this type of window is challenging due to the multiple interfaces and complex scattering effects that they introduce. Exterior-facing windows are typically designed to have low-E properties with multiple panes for energy efficiency to prevent heat from entering and escaping the interior. Both of these properties make RF penetration particularly challenging, so the specific type of glass that was chosen represents the most lossy class of windows that may be encountered in practical scenarios. See Figures 9 and 10, below.

"Glass #2" is a simple single pane clear glass that may be typical of glass installed indoors without an interface to the outside environment. The thickness is 6.35 mm (1/4"). This glass

type represents the other end of the spectrum; it is relatively simple to penetrate with poor reflectivity. See Figure

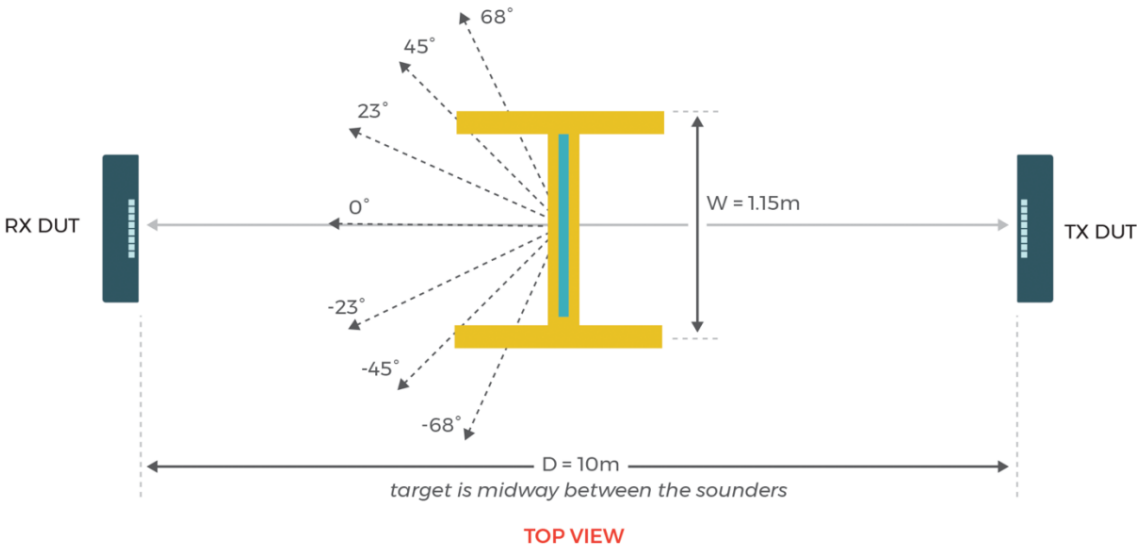

Figure 7: Diagram showing definition of incidence angles and relative position and dimensions of Glass #1 measurement

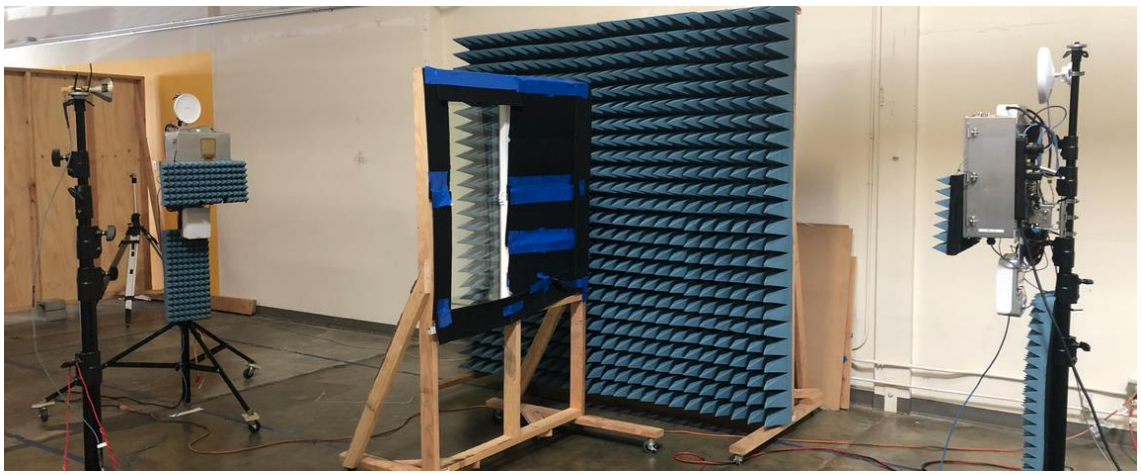

Figure 8: Photograph of the measurement setup with Glass #1. Absorbent foam sheets are used to cover the window frame to prevent any unwanted reflections and interference

Penetration through Glass #1 could only be reliably reported for a normal incidence angle, since the window size was too small to allow a sufficiently large aperture given the beam width of the two radios. See Table 8 for summary results.

	60GHz		28GHz	
Description	**# of Samples**	**Loss (dB)**	**# of Samples**	**Loss (dB)**
Glass #1 - incident angle 0°	4	33.2 ± 3.7	4	27.4 ± 4.0

Table 8: Penetration loss for normal incidence angle through Glass #1

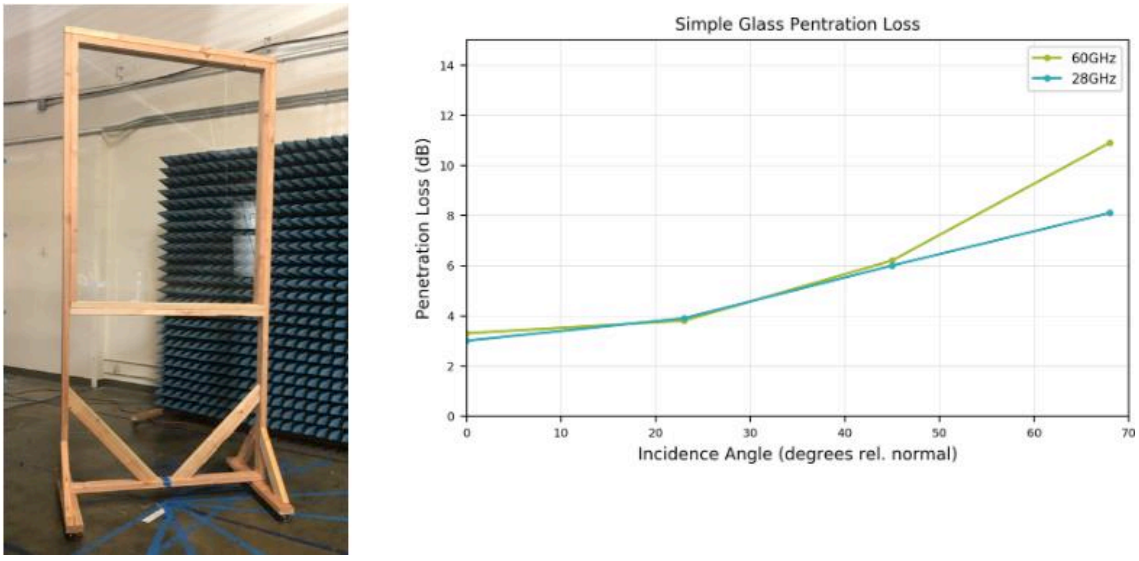

Figure 9: Photograph of Glass #2 with graph of loss as a function of incidence angle

	60GHz		28GHz	
Description	**# of Samples**	**Loss (dB)**	**# of Samples**	**Loss (dB)**
Glass #2 - incident angle 0°	2	3.3 ± 0.7	2	3.0 ± 0.7
Glass #2 - incident angle 23°	4	3.8 ± 0.5	4	3.9 ± 0.3
Glass #2 - incident angle 45°	4	6.2 ± 0.5	4	6.0 ± 0.4
Glass #2 - incident angle 68°	4	10.9 ± 0.5	4	8.1 ± 0.3

Table 9: Glass #2 penetration losses with different incident angles

The measurements for Glass #2 taken in this study (see Figure 11 and Table 9, above) compare well to the findings of other campaigns, although somewhat higher at 28GHz. In "28GHz millimeter wave cellular communication measurements for reflection and penetration loss in and around buildings in New York city," [4] Zhao *et al* conducted penetration loss measurements and found that clear glass induces attenuation of 3dB/cm and tinted glass induces attenuation of 19dB/cm. Choi *et al* measured the average penetration loss of glass

from 13GHz to 28GHz to be 1dB in "Characteristics Analysis of Reflection and Transmission According to Building Materials in the Millimeter Wave Band". In "Propagation Characterization of an Office Building in the 60GHz Band" [3], Lu et al found that the propagation loss of clear glass was equivalent to 4.3dB/cm at 60GHz. Huang *et al* measured a transmission loss of 4.0dB/cm at 60GHz for tempered glass in "60GHz Transmission and Reflection Measurements" [7].

It is interesting to note that there has been relatively little investigation of the propagation loss of low-emissivity (low-E) glass prior to this study in spite of its pervasiveness.

5.4 Foliage

Penetration measurements were made for three types of trees, categorized here as Dense Foliage, Medium-Density Foliage, and Sparse Foliage (see Figure 12). All trees used are approximately 2m in height, and 0.5m to 1m in thickness. Since distribution of density in all three types of foliage is difficult to quantify, many measurements were taken at a variety of orientations and positions relative to the LOS. While it is impossible to ensure that both the 60GHz and 28GHz radios are transmitting through the same spot in the tree, through averaging over many positions an average loss value can be established and is representative of losses that may typically be encountered.

Figure 10: Three foliage types evaluated in penetration experiments: (a) Dense Foliage (White Cedar), (b) Medium-Density Foliage (Photinia), (c) Sparse Foliage (Oleander)

For each type of foliage, measurements were taken with varying levels of LOS blockage, starting from the extreme edge, where LOS is completely unobstructed, to the other, unobstructed edge. In this way, we can characterize the loss profile of each tree while also capturing the maximum loss value encountered. These numbers can be extrapolated to all other tree thicknesses of similar densities as a loss per meter.

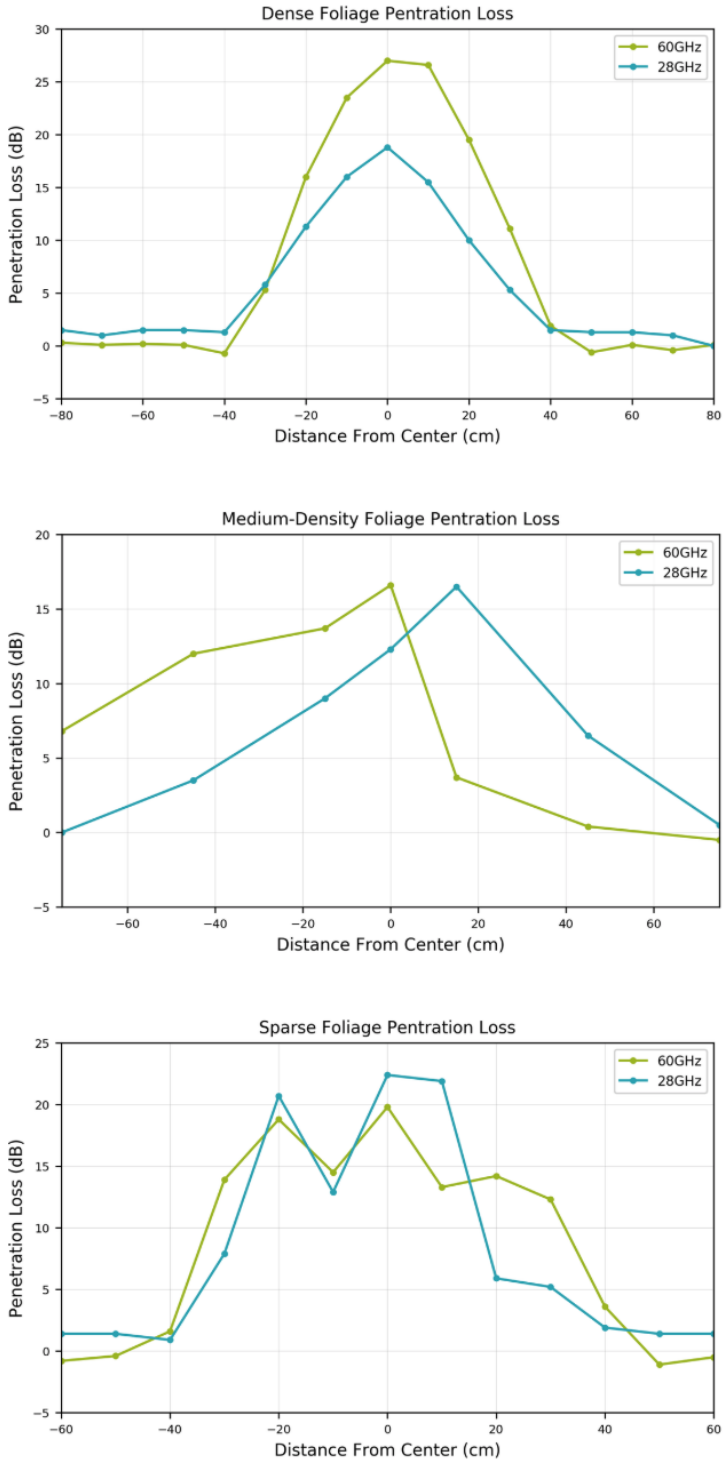

Figure 11: Penetration losses for the three different foliage types

	60GHz		28GHz	
Description	**# of Samples**	**Loss (dB)**	**# of Samples**	**Loss (dB)**
Dense Foliage: 80 cm from center	2	0.1 ± 0.4	2	0.0 ± 0.7
Dense Foliage: 70 cm from center	2	-0.4 ± 0.3	2	1.0 ± 0.7
Dense Foliage: 60 cm from center	2	0.1 ± 0.3	2	1.3 ± 1.1
Dense Foliage: 50 cm from center	2	-0.6 ± 0.7	2	1.3 ± 0.4
Dense Foliage: 40 cm from center	3	1.9 ± 0.4	2	1.5 ± 0.0
Dense Foliage: 30 cm from center	3	11.1 ± 0.3	2	5.3 ± 0.4
Dense Foliage: 20 cm from center	3	19.5 ± 0.3	2	10.0 ± 0.0
Dense Foliage: 10 cm from center	3	26.6 ± 0.4	2	15.5 ± 0.0
Dense Foliage: center	**4**	**27.0 ± 0.4**	**2**	**18.8 ± 0.4**
Dense Foliage: -10 cm from center	3	23.5 ± 0.4	2	16.0 ± 0.0
Dense Foliage: -20 cm from center	3	16.0 ± 0.6	2	11.3 ± 0.4
Dense Foliage: -30 cm from center	3	5.3 ± 0.5	2	5.8 ± 0.4
Dense Foliage: -40 cm from center	2	-0.7 ± 0.0	2	1.3 ± 0.4
Dense Foliage: -50 cm from center	2	0.1 ± 0.4	2	1.5 ± 0.0
Dense Foliage: -60 cm from center	2	0.2 ± 0.2	2	1.5 ± 0.7
Dense Foliage: -70 cm from center	2	0.1 ± 0.4	2	1.0 ± 0.7
Dense Foliage: -80 cm from center	2	0.3 ± 0.0	2	1.5 ± 0.0

Table 10: Dense foliage penetration loss as a function of distance from center

	60GHz		28GHz	
Description	**# of Samples**	**Loss (dB)**	**# of Samples**	**Loss (dB)**
Med-density Foliage: 75 cm from center	1	-0.5	1	0.5
Med-density Foliage: 45 cm from center	1	0.4	1	6.5
Med-density Foliage: 15 cm from center	1	3.7	1	16.5
Med-density Foliage: center	**6**	**16.6 ± 4.5**	**6**	**12.3 ± 4.4**
Med-density Foliage: -15 cm from center	1	13.7	1	9
Med-density Foliage: -45 cm from center	1	12	1	3.5
Med-density Foliage: -75 cm from center	1	6.8	1	0

Table 11: Medium-density foliage penetration loss as a function of distance from center

	60GHz		28GHz	
Description	**# of Samples**	**Loss (dB)**	**# of Samples**	**Loss (dB)**
Sparse Foliage: 60 cm from center	2	-0.5 ± 0.9	2	1.4 ± 0.7
Sparse Foliage: 50 cm from center	2	-1.1 ± 1.3	2	1.4 ± 0.0
Sparse Foliage: 40 cm from center	2	3.6 ± 1.1	2	1.9 ± 0.0

Sparse Foliage: 30 cm from center	2	12.3 ± 1.2	2	5.2 ± 1.1
Sparse Foliage: 20 cm from center	2	14.2 ± 0.2	2	5.9 ± 0.7
Sparse Foliage: 10 cm from center	2	13.3 ± 0.2	2	21.9 ± 1.4
Sparse Foliage: center	**4**	**19.8 ± 1.2**	**2**	**22.4 ± 0.7**
Sparse Foliage: -10 cm from center	2	14.5 ± 0.6	2	12.9 ± 1.4
Sparse Foliage: -20 cm from center	4	18.8 ± 2.1	2	20.7 ± 1.1
Sparse Foliage: -30 cm from center	2	13.9 ± 0.3	2	7.9 ± 0.7
Sparse Foliage: -40 cm from center	2	1.6 ± 0.5	2	0.9 ± 0.7
Sparse Foliage: -50 cm from center	2	-0.4 ± 1.0	2	1.4 ± 0.0
Sparse Foliage: -60 cm from center	2	-0.8 ± 1.0	2	1.4 ± 0.0

Table 12: Sparse foliage penetration loss as a function of distance from center

Table 12 summarizes the measurements that were performed along with the average measured penetration loss with standard deviation.

Given the non-uniform distribution of material over the cross section of a tree and the wide variety of tree foliage, it is difficult to directly compare the results obtained in this study with those found in the literature. It should be noted that penetration loss *per meter* measured across a single tree specimen is an order of magnitude higher than that measured across a cluster of trees in a wood or forest, due to the concentration of foliage around the trunk and open air in between.

In "Foliage Attenuation Measurement at Millimeter Wave Frequencies in Tropical Vegetation", Rahim *et al* reported a penetration loss of 8.8dB/m at 28GHz. In "Attenuation by a Human Body and Trees as well as Material Penetration Loss in 26 and 39GHz Millimeter Wave Bands", Wang *et al* reported up to 18dB penetration loss for a single tree.

In "Millimeter Wave Propagation: Spectrum Management Implications" [12], the FCC endorses the penetration loss model through foliage developed in CCIR Report 236-2:

$$L = 0.2 * f^{0.3} * R^{0.6} \; [units \; in \; dB]$$

where f is frequency in MHz, R is depth of foliage transversed in meters, and applies for $R < 400m$. The model gives ~5.4dB at one meter at 60GHz and ~4.2dB at one meter at 20GHz. The results are comparable with the measurements obtained in this study when averaged across the tree span.

6. Reflection Loss Measurements

An understanding of losses through reflections from common construction materials would allow network operators to deploy mmWave networks more intelligently. In environments where LOS links may be unexpectedly blocked, such as in environments with lots of street foliage, the use of building reflections can allow secondary NLOS link paths. In other circumstances where interference between radios may be problematic, deploying in environments with many natural reflectors should be avoided.

Both transmission and reflection losses are highly dependent on incident angle as governed by the Fresnel equations. All reported measurements for reflection are made at a 45° incident angle, with a distance of 3m between the reflecting surface and each radio. The reference path loss for both units are the measured at a distance of 6m, so that absolute reflection loss is the difference between the total loss over 6m with a reflector, and over 6m of free space without a reflector.

Reflection loss measurements were completed for the low-E double-pane window glass (Glass #1). An absorbent foam was used to cover all non-glass reflective surfaces, such as the frame of the window, to prevent capturing reflections from other materials. Additionally, an absorbent foam wall was placed behind the window, so that all transmitted energy was not reflected back to interfere with the measurement. The reflection measurements at different incident angles for Glass #1 are shown in Figure 14, below.

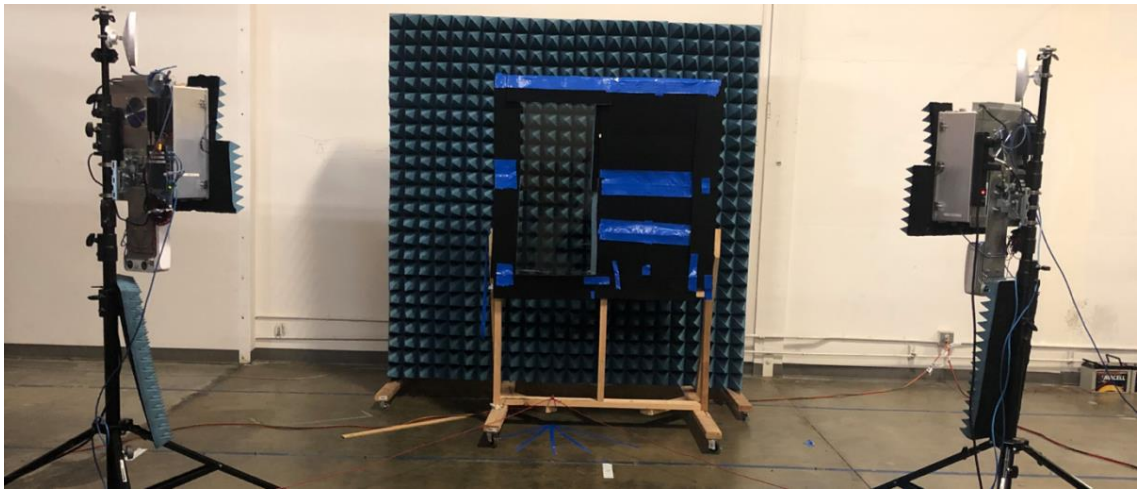

Figure 12: Photograph of measurement setup for reflection through Glass #1. Non-glass reflective surfaces and the backside of the glass are covered with an RF absorbent foam to prevent reflections from other materials

"Glass #2" is a simple single pane clear glass that may be typical of glass installed indoors without an interface to the outside environment. The reflection losses for both Glass #1, Glass #2, concrete, wood, and drywall at an incident angle of 45 degrees is shown in Table 13, below.

	60GHz		28GHz	
Description	**# of Samples**	**Loss (dB)**	**# of Samples**	**Loss (dB)**
Glass #1 - incident angle 45°	4	8.4 ± 0.6	4	10.2 ± 3.0
Glass #2 - incident angle 45°	6	2.0 ± 0.2	6	0.4 ± 0.4
Concrete - incident angle 45°	6	5.7 ± 0.7	6	4.7 ± 0.3
Wood - incident angle 45°	6	6.6 ± 0.5	6	5.8 ± 1.0
Drywall - incident angle 45°	6	13.5 ± 1.3	6	4.2 ± 1.3

Table 13: Summary of all reflection measurements at a 45° incident angle (distance of 3m from surface to each radio)

The general observation from these measurements is that the reflection losses at 28GHz are moderately less than the losses at 60GHz. In the case of Glass #2 and Drywall, the difference in losses is statistically significant and much greater than the standard deviation between measurements. For the case of concrete and wood, the differences between mean reflection losses are within the range of measurement errors and variations.

One unexpected observation is reflection loss for glass #1, where losses at 28GHz were greater than 60GHz. Additionally, reflection loses at both bands is larger than Glass #2, which is unexpected since Glass #1 has a conductive coating that should result in less reflection loss. One possible reason for this error in measurement is the small aperture of the glass surface at an angle, resulting in partial blockage within the Fresnel zone and only partial reflection of the transmitted beam.

Comparing the losses to those reported in literature, we see fairly close alignment. Reflection losses over 13GHz to 28GHz were measured by Choi *et al* in "Characteristics Analysis of Reflection and Transmission According to Building Materials in the Millimeter Wave Band" [9]. The absolute reflection losses at a 45° incidence angle were found to be 3.5dB for glass, 6.1dB for concrete, 19.5dB and 11.6dB for wood and plywood respectively, and 11.29 for drywall. Zhao *et al* measured reflection losses at 28GHz in "28GHz Millimeter Wave Cellular Communication Measurements for Reflection and Penetration Loss in and around Buildings in New York City" [4]. These were found to be 0.95dB for tinted glass at a 10° incidence, 2.6dB for clear glass at 10° incidence, 4.1dB for concrete at 45° incidence, and 4.0dB for drywall at 45° incidence. Lu *et al* measured complex relative permittivity of common materials at 60GHz

in “Propagation Characterization of an Office Building in the 60GHz Band” [3]. Using the permittivity measurements to calculate reflection losses at 45°, the losses from drywall, drywall with semi-gloss paint, drywall with flat paint and backer board are 3.7dB, 3.0dB, 5.0dB and 4.1dB respectively. The reflection losses for glass were 1.9dB and the losses for wood were 6.4dB, which is a very close match to measurements reported in this paper for Glass #2 and wood.

7. Summary

The losses associated with mmWave links relying on penetration and reflection through common building materials were measured and characterized in a side-by-side study from the 28GHz and 60GHz bands. The average transmission and reflection losses are summarized in Table 14, below:

	Penetration (0°)		Reflection (45°)	
	60GHz	28GHz	60GHz	28GHz
Description	Loss (dB)	Loss (dB)	Loss (dB)	Loss (dB)
Complex Glass *(glass #1)*	33.2	27.4	8.4	10.2
Simple Glass *(glass #2)*	3.3	3	2	0.4
Concrete	-	-	5.7	4.7
Foliage (peak loss over 3 types)	21.1	19.2	-	-
Wood (average in dB/cm over 3 types)	4.7	2.9	6.6	5.8
Drywall (dB/layer)	1.2	0.8	13.5	4.2

Table 14: Summary of all penetration losses (at normal 0° incidence) and reflection losses (at 45° incidence angle)

As expected, losses through typical building glass (double pane and low-E) are very large in both bands due to the conductive coating, multiple interfaces, and complex scattering properties. The losses for simple single-pane glass were an order of magnitude lower in both bands. In conclusion, both reflection and penetration loss through glass is highly dependent on glass type and geometry, but is generally uniform between both of the mmWave bands that were studied.

Losses through foliage were observed to be significant in both bands, with no clear advantage to either band. While transmission losses are highly dependent on the type and density of foliage, communication through dense foliage with the observed worst-case losses is possible if tradeoffs in the network design are made to reduce the link distance or the data rate. Links deployed in environments where LOS is likely to be blocked by foliage should provide an adequate link budget to offset the large potential losses.

Reflection losses for typical wall materials (concrete, wood, and drywall) are observed to be at least 1dB less in the 28GHz band, but losses in both bands are sufficiently small that reflections through these materials can be utilized for NLOS communication. Transmission losses through wood and drywall are observed to be similarly small in magnitude, with a slight advantage in the 28GHz band. While typical wall constructions include more layers than simple wood and drywall compositions, these measurements indicate a strong potential for using both mmWave bands for LOS communication through interior wall constructions.

In conclusion, despite the challenges faced by technologies operating in the mmWave spectrum, when transmitting though lossy channels link budgets can account for known losses and reliable links can be deployed when these factors are considered.

This study presents a detailed understanding of mmWave signal propagation in an indoor environment and can be used for link budget preparation and network planning for indoor applications of the mmWave technology. As a follow-up to this study, the group plans use the same setup of 28GHz and 60GHz channel sounders and conduct experiments in an outdoor environment under conditions experienced by typical outdoor deployments of the mmWave technology. This follow-up study is aimed to be released around October 2019.

Contact Info

WEBSITE
https://telecominfraproject.com

EMAIL
membership@telecominfraproject.com

References

[1] Telecom Infra Project (TIP) Website: https://telecominfraproject.com/

[2] TIP mmWave Project Group Website: https://mmwave.telecominfraproject.com/

[3] Propagation characterization of an office building in the 60GHz band; Jonathan Lu, Daniel Steinbach, Patrick Cabrol, Phil Pietraski, Ravikumar V. Pragada, The 8th European Conference on Antennas and Propagation (EuCAP 2014)

[4] "28GHz millimeter wave cellular communication measurements for reflection and penetration loss in and around buildings in New York city"; Hang Zhao, Rimma Mayzus, Shu Sun, Mathew Samimi, Jocelyn K. Schulz, Yaniv Azar, Kevin Wang, George N. Wong, Felix Gutierrez, Theodore S. Rappaport; 2013 IEEE International Conference on Communications (ICC)

[5] "In-Building Wideband Partition Loss Measurements at 2.5GHz and 60GHz"; Christopher R. Anderson and Theodore S. Rappaport; IEEE Transactions on Wireless Communications, VOL. 3, NO. 3, May 2004

[6] "Millimeter Wave Propagation: Spectrum Management Implications"; Federal Communications Commission; Office of Engineering and Technology; Bulletin Number 70; July 1997

[7] "60GHz Transmission and Reflection Measurements"; Tian-Wei Huang, Wen-Heng Lin, Jian-Zhong Lo, Xun Lan, James Wang, Vish Ponnampalam, Alvin Hsu; IEEE 802.11-09/0995r1

[8] Terragraph by Facebook: https://terragraph.com/

[9] "Characteristics Analysis of Reflection and Transmission According to Building Materials in the Millimeter Wave Band."; Choi, Byeong-Gon et al.; Recent Advances on Electroscience and Computers (2015); ISBN: 978-1-61804-290-3

[10] “Item level characterization of mm-wave indoor propagation”; F. Fuschini, S. Häfner, M. Zoli, R. Müller, E. M. Vitucci, D. Dupleich, M. Barbiroli, J. Luo, E. Schulz, V. Degli-Esposti and R. S. Thomä; EURASIP Journal on Wireless Communications and Networking; 2016

[11] “5G Channel Model for bands up to 100GHz”; Aalto University, AT&T, BUPT, CMCC, Ericsson, Huawei, INTEL, New York University, Nokia, NTT DOCOMO, Qualcomm, Samsung, University of Bristol, University of Southern California; Revision 2.2; September 2016

[12] “Foliage Attenuation Measurement at Millimeter Wave Frequencies in Tropical Vegetation”; Hairani Maisarah Rahim, Chee Yen Leow, Tharek Abd Rahman, Arsany Arsad and Muhammad Arif Malek Wireless Communication Centre, Faculty of Electrical Engineering, Universiti Teknologi Malaysia; 2017 IEEE 13th Malaysia International Conference on Communications (MICC), 28-30 Nov. 2017

[13] “Attenuation by a Human Body and Trees as well as Material Penetration Loss in 26 and 39GHz Millimeter Wave Bands”; Qi Wang[1], Xiongwen Zhao[1,2,3], Shu Li[1], Mengjun Wang[2], Shaohui Sun[2], Wei Hong[3]; International Journal of Antennas and Propagation, Volume 2017, Article ID 2961090

1. School of Electrical and Electronic Engineering, North China Electric Power University, Beijing 102206, China
2. State Key Laboratory of Wireless Mobile Communications, China Academy of Telecommunications Technology (CATT), Beijing 100191, China
3. State Key Laboratory of Millimeter Wave, Southeast University, Nanjing 210096, China

[14] Esencia Technologies, Inc

Abbreviations

3GPP	3rd Generation Partnership Project
5G NR	5th Generation – New Radio
ADC	Analog-to-Digital Convertor
BBIC	Baseband Integrated Circuit
dB	Decibel
dBm	Decibel in milliwatts
DUT	Device Under Test
EIRP	Effective Isotropic Radiated Power
FSPL	Free Space Path Loss
IEEE	Institute of Electrical and Electronics Engineers
IF	Intermediate Frequency
LOS	Line of Sight
Low-E	Low Emissivity

LUT	Lookup Table
MCS	Modulation and Coding Scheme
mmWave	Millimeter Wave
NI	National Instruments
NLOS	Non-Line-of-Sight
OSB	Oriented Strand Board
P2MP	Point to Multi-Point
PA	Power Amplifier
PCB	Printed Circuit Board
PL	Pathloss
RF	Radio Frequency
RFIC	RF Integrated Circuit
RSSI	Received Signal Strength Indicator
RX	Receiver
TG	Terragraph by Facebook
TIP	Telecom infra project
TX	Transmitter
VSA	Vector Signal Analyzer

TIP Document License

By using and/or copying this document, or the TIP document from which this statement is linked, you (the licensee) agree that you have read, understood, and will comply with the following terms and conditions:

Permission to copy, display and distribute the contents of this document, or the TIP document from which this statement is linked, in any medium for any purpose and without fee or royalty is hereby granted under the copyrights of TIP and its Contributors, provided that you include the following on ALL copies of the document, or portions thereof, that you use:

1. A link or URL to the original TIP document.
2. The pre-existing copyright notice of the original author, or if it doesn't exist, a notice (hypertext is preferred, but a textual representation is permitted) of the form: "Copyright 2019, TIP and its Contributors. All rights Reserved "
3. When space permits, inclusion of the full text of this License should be provided. We request that authorship attribution be provided in any software, documents, or other items or products that you create pursuant to the implementation of the contents of this document, or any portion thereof.

No right to create modifications or derivatives of TIP documents is granted pursuant to this License. except as follows: To facilitate implementation of software or specifications that may be the subject of this document, anyone may prepare and distribute derivative works and portions of this document in such implementations, in supporting materials accompanying the implementations, PROVIDED that all such materials include the copyright notice above and this License. HOWEVER, the publication of derivative works of this document for any other purpose is expressly prohibited.

For the avoidance of doubt, Software and Specifications, as those terms are defined in TIP's Organizational Documents (which may be accessed at https://telecominfraproject.com/organizational-documents/), and components thereof incorporated into the Document are licensed in accordance with the applicable Organizational Document(s).

Disclaimers

THIS DOCUMENT IS PROVIDED "AS IS," AND TIP MAKES NO REPRESENTATIONS OR WARRANTIES, EXPRESS OR IMPLIED, INCLUDING, BUT NOT LIMITED TO, WARRANTIES OF MERCHANTABILITY, FITNESS FOR A PARTICULAR PURPOSE, NON-INFRINGEMENT, OR TITLE; THAT THE CONTENTS OF THE DOCUMENT ARE SUITABLE FOR ANY PURPOSE; NOR THAT THE IMPLEMENTATION OF SUCH CONTENTS WILL NOT INFRINGE ANY THIRD PARTY PATENTS, COPYRIGHTS, TRADEMARKS OR OTHER RIGHTS.

TIP WILL NOT BE LIABLE FOR ANY DIRECT, INDIRECT, SPECIAL OR CONSEQUENTIAL DAMAGES ARISING OUT OF ANY USE OF THE DOCUMENT OR THE PERFORMANCE OR IMPLEMENTATION OF THE CONTENTS THEREOF.

The name or trademarks of TIP may NOT be used in advertising or publicity pertaining to this document or its contents without specific, written prior permission. Title to copyright in this document will at all times remain with TIP and its Contributors.

This TIP Document License is based, with permission from the W3C, on the W3C Document License which may be found at https://www.w3.org/Consortium/Legal/2015/doc-license.html.